J. Fluid Mech. (1979), *vol.* 93, *part* 1, *pp.* 47–63
Printed in Great Britain

Experiments on the Weis-Fogh mechanism of lift generation by insects in hovering flight. Part 1. Dynamics of the 'fling'

By T. MAXWORTHY

Departments of Mechanical and Aerospace Engineering, University of Southern California, Los Angeles, California 90007

(Received 21 March 1978 and in revised form 9 October 1978)

From a series of experiments using simplified mechanical models we suggest certain minor modifications to the Weis-Fogh (1973)–Lighthill (1973) explanation of the so-called 'clap and fling' mechanism for the generation of large lift coefficients by insects in hovering flight. Of particular importance is the production and motion of a leading edge, separation vortex that accounts for virtually all of the circulation generated during the initial phase of the 'fling' process. The magnitude of this circulation is substantially larger than that calculated using inviscid theory. During the motion that subsequently separates the wings, the vorticity over each of them is convected and combined to become a tip vortex of uniform circulation spanning the space between them. This combined vortex moves downwards as a part of a ring, of large impulse, that is then continuously fed from quasi-steady separation bubbles that move with the wings as they continue to open at a large angle of attack. Such effects are able to account for the large lift forces generated by the insect.

1. Introduction

Weis-Fogh (1973) and Lighthill (1973) have devised an ingenious explanation for the fluid–dynamic processes whereby certain insects are able to generate large lift coefficients by use of the so-called 'clap and fling' mechanism. They give particular emphasis to the 'fling' portion of the motion and in the present paper we follow this tradition and show how real fluid effects modify the inviscid argument put forth by these two authors and as partly anticipated in the latter paper. However, in subsequent parts we hope to show that both the 'clap' and the 'flip' phases and interaction effects are also important and account for much of the total impulse applied to the fluid by the insect during each cycle of wing motion.

The overall problem, originally outlined by Weis-Fogh (1973), has been extended and reviewed by Lighthill (1973, 1975) and modified by Ellington (1975) so that the basic motion of the wing surfaces seems clear, although some previously unrevealed and important subtleties will be discussed in § 2. Starting at the instant in time when both wing surfaces are pressed together, the 'fling' stage consists of an opening of the wings by rotation about their bottom edges until the including angle between them is about 120° at which time they begin to move apart in an arc centred at the wing root at the body of the insect (see figure 1). Although this process was originally discussed for the small wasp *Encarsia formosa*, it now appears that larger insects use

0022-1120/79/4255-6870 $02.00

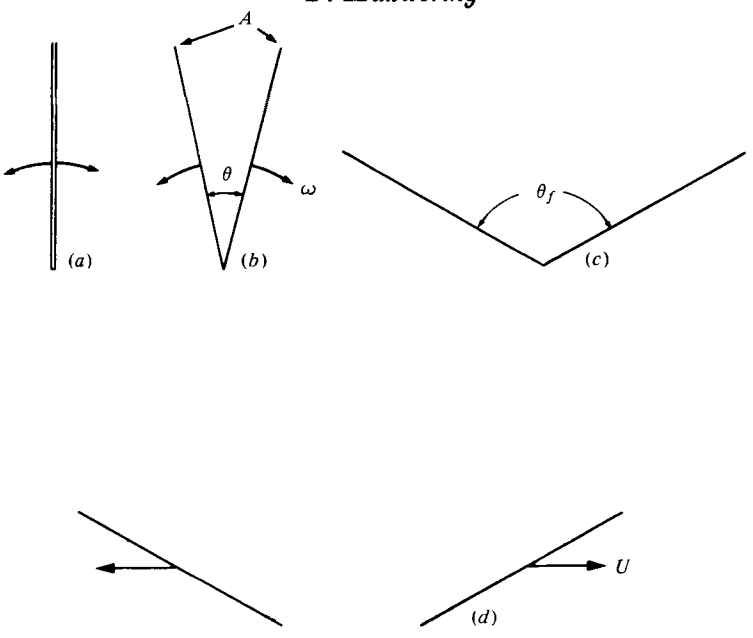

FIGURE 1. Diagrammatic view of wing motion in 'fling' mode. After Lighthill (1973). (*a*), (*b*) and (*c*) show the initial phase of the 'fling', the sequence forms the basis for the experimental apparatus of figure 3. (*d*) Second phase of the 'fling'.

the same processes (Ellington, private communication) so that a wide range of Reynolds numbers (Re) is encompassed in nature from values as low as 20 to values at least as large as 200. (Here $Re = \dot{\omega}c_0^2/\nu$ and $\dot{\omega}/s$ is the rotation rate of the surface, c_0 a maximum chord length and ν the kinematic viscosity of the ambient fluid.) The initial stages of this process, i.e. the wing rotation about a common axis, figures 1 (*a*)–(*c*), also appears to be typical of a large group of insects of which the *Papilionoidea* or butterflies are probably the most notable. In this sub-order, the insect's dimensions and the wing flapping rates can be substantial, resulting in values of Re as large as 5×10^3; while the final angle, θ_f in figure 1 (*c*), is typically 270–360°.

In Lighthill's (1973) theoretical description of these processes, a two-dimensional, inviscid model of the wing opening process was considered, in his § 2. The inrush of air into the opening gap corresponds to an initially infinite circulation (Γ) around a single wing which falls, as the wings open, to a minimum value of $0{\cdot}69\,\dot{\omega}c^2$ when $\theta = 180°$ (see figure 7). It was hypothesized that at some intermediate stage, when $\theta \approx 120°$, Γ is slightly larger than the quoted minimum value and as the wings begin to part with velocity U, that a lift corresponding to $\rho U\Gamma$/unit length is immediately developed without the need to continuously shed trailing vorticity and for the lift to build slowly to its asymptotic value as in the classical problem of an impulsively started single wing calculated by Wagner (1925). It was pointed out that the lift in the subsequent horizontal motion of both aerofoils depends only on the circulation around each; also that such circulation about one aerofoil generates a downwash at the other which reduces its effective angle of attack below the apparently very large geometrical angles of attack which are observed.

Section 3 of the same paper gave a lengthy discussion of the viscous effects that must be expected to modify the pattern described above. The certainty that they must

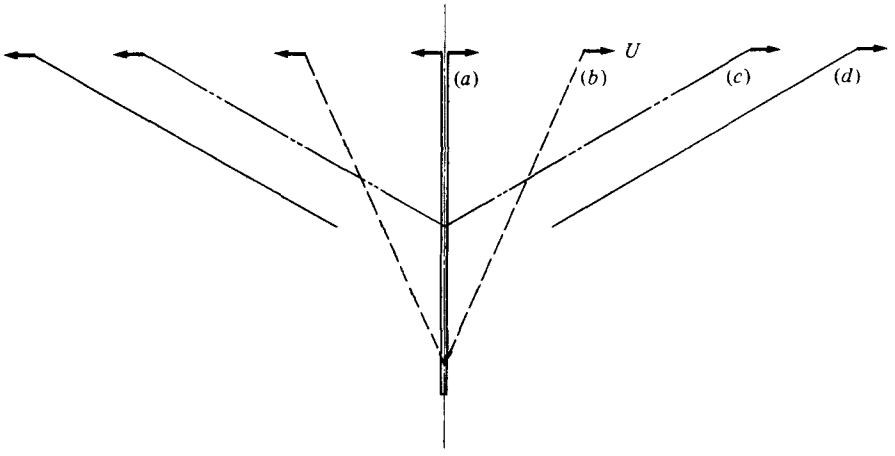

FIGURE 2. Another possible sequence of wing motion in which the leading edges of the wings move in an horizontal plane and the axis of rotation moves upwards. This sequence forms the basis for the motion of the wings in the experimental apparatus shown in figure 4.

involve a leading-edge separation which will slightly enhance the overall circulation was emphasized. Section 4 was concerned with embedding the two-dimensional-aerofoil treatment into an overall three-dimensional picture of the flow around the hovering insect, emphasizing that the weight of the insect would be balanced by the impulse of a chain of downward-moving vortex rings, which at large distances below the insect would, at its Reynolds number, be merged by the action of viscous effects into a laminar jet-like motion. Those suggestions anticipate to a certain extent the findings of this paper, although the latter are much more precise and quantitative and are demonstrated with clear model experiments.

In § 2 we describe the models used to unravel features of the flow around wings moving in a real, viscous fluid; in § 3 the results are described while in § 4 we discuss the consequences of these results and use a simple order of magnitude argument to calculate the forces involved.

2. Apparatus and procedure

In the present case, the design of models to simulate insect wing motion is hampered by an inexact knowledge of the precise details of such motion. In particular, during the initial opening phase it is not clear whether the motion is simply a rotation about an axis fixed in space (figures 1*a*, *b*) as modelled in the theory, or if a simultaneous vertical rise of the axis is also involved (figure 2). Such a vertical excursion would be created if the wing opening were caused by a simple translation of the leading edge in such a way that trailing edges were forced together by fluid dynamical forces thus produced. Also, if the lift forces substantially exceeded the insect weight the insect itself would accelerate upwards lifting the axis of rotation at the same time. From published accounts both horizontal and vertical movement of the wing leading edge appears to be involved during some phases of the total cycle, however, in the two models to be described we have considered the two extremes mainly for reasons of mechanical simplicity but also to see how sensitive the flow pattern is to the exact details of overall vertical motion. We also believe that the flexibility of the insects'

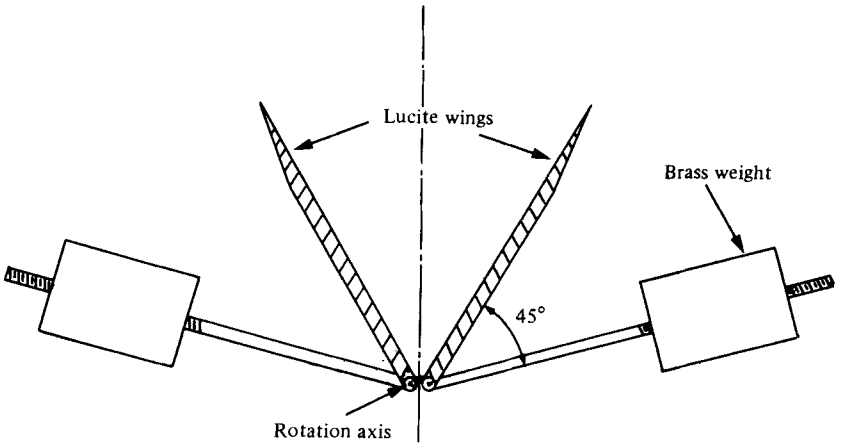

FIGURE 3. Apparatus to study two-dimensional flow over rotating wings. The chord is 10 cm, the wings 30 cm long and are placed between end walls to avoid three-dimensional flows.

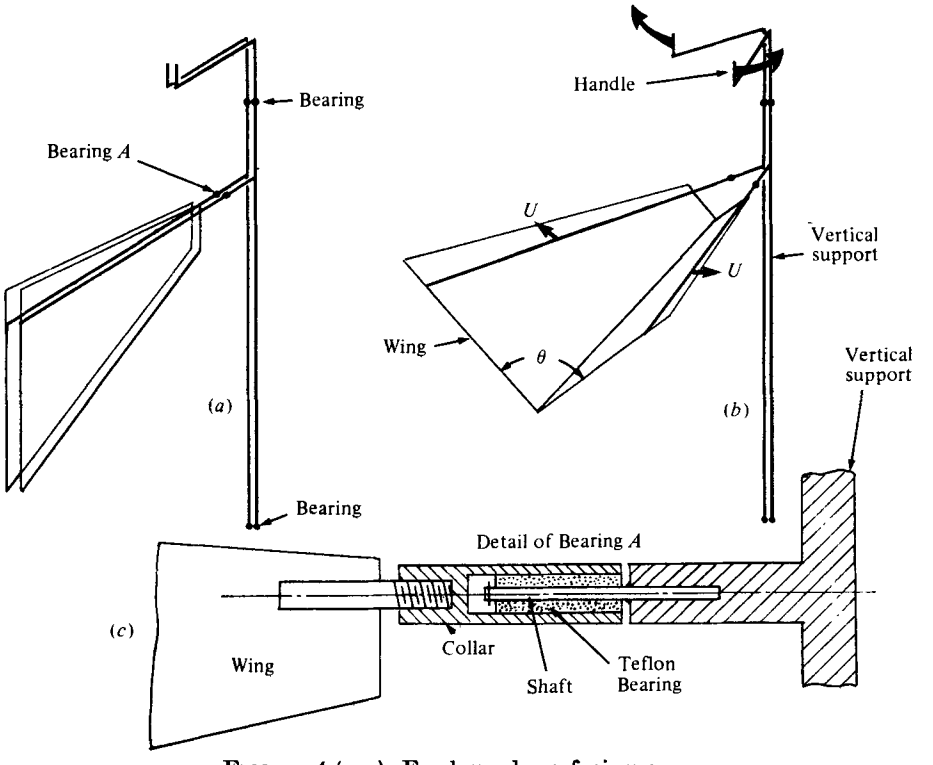

FIGURE 4 (a–c). For legend see facing page.

wings, and their subsequent response to the forces applied to them, modify the flow pattern over the wing and thus, in turn, change the forces. Because of the greater complexity introduced by this possibility, and because even the grossest features of the flow are not known, we have postponed discussion of this complication to a later paper and will only consider the flow due to inflexible wings in what follows. We also ignore the effects of downwash due to vorticity produced during previous wing motions.

The first model (figure 3) was made to simulate the two-dimensional theory as

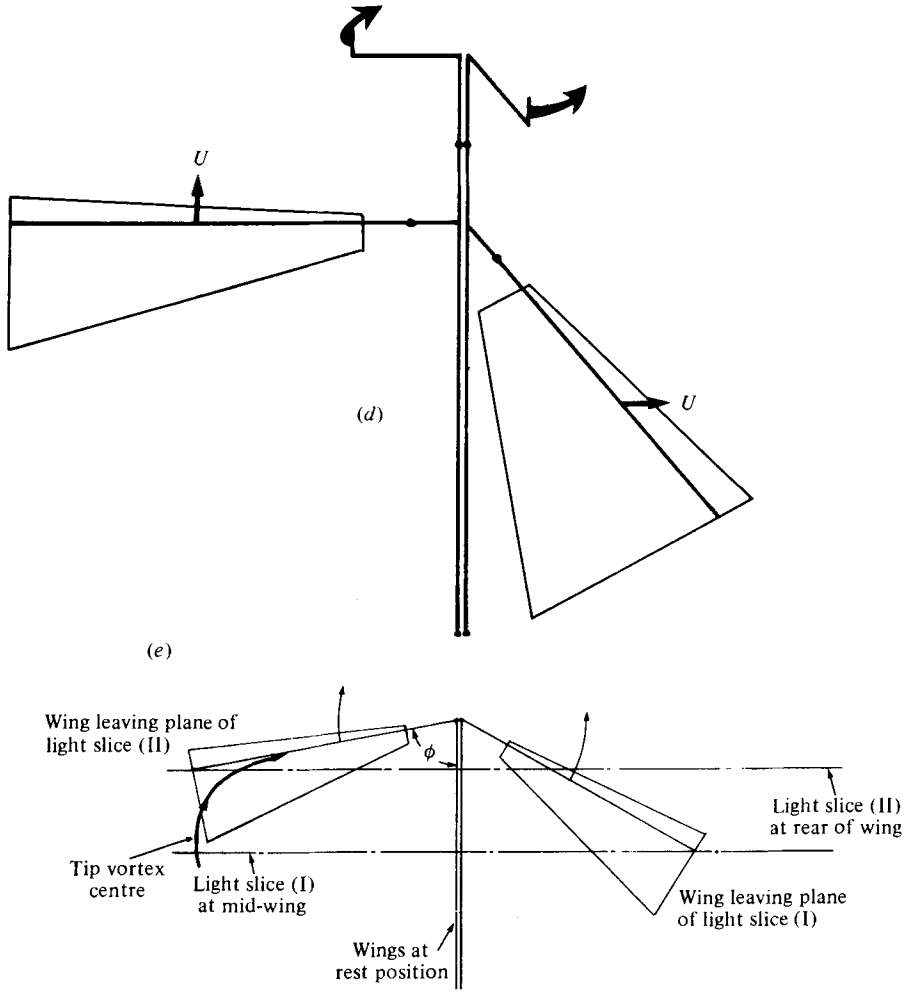

FIGURE 4. (*a*, *b*, *d*) Diagrams showing the mode of operation of the three-dimensional model. The apparatus is operated by hand. Details of the main wing bearing are shown in (*c*) but the devices that stop the wings at a fixed angle of attack have been omitted for the sake of clarity. (*e*) Shows a plan view of this apparatus and locates the light planes used to illuminate small wax particles in the fluid. The wings are shown leaving the light planes in order to show that the ultimate flow picture will be of the tip vortices.

closely as possible and it is, in fact, a modification of an initial one that used only one wing and a solid wall at the plane of symmetry. This latter model gave some interesting flow patterns resulting from boundary layer separation at the stationary wall. In order to avoid such problems, a symmetric model was built with two wings that could be released from rest from any initial angle (θ_i). With the counterweights fixed into the position shown in figure 3 the rate of wing opening was almost constant once the wings had opened through a small angle.

The second model (figure 4) is considerably more complex in its mode of operation since we wished to observe the effects of the three-dimensionality of the flow field. This model simulates the wings motion of the real insect very closely, but perhaps not closely enough. The vertical body of the insect is replaced by two vertical rods

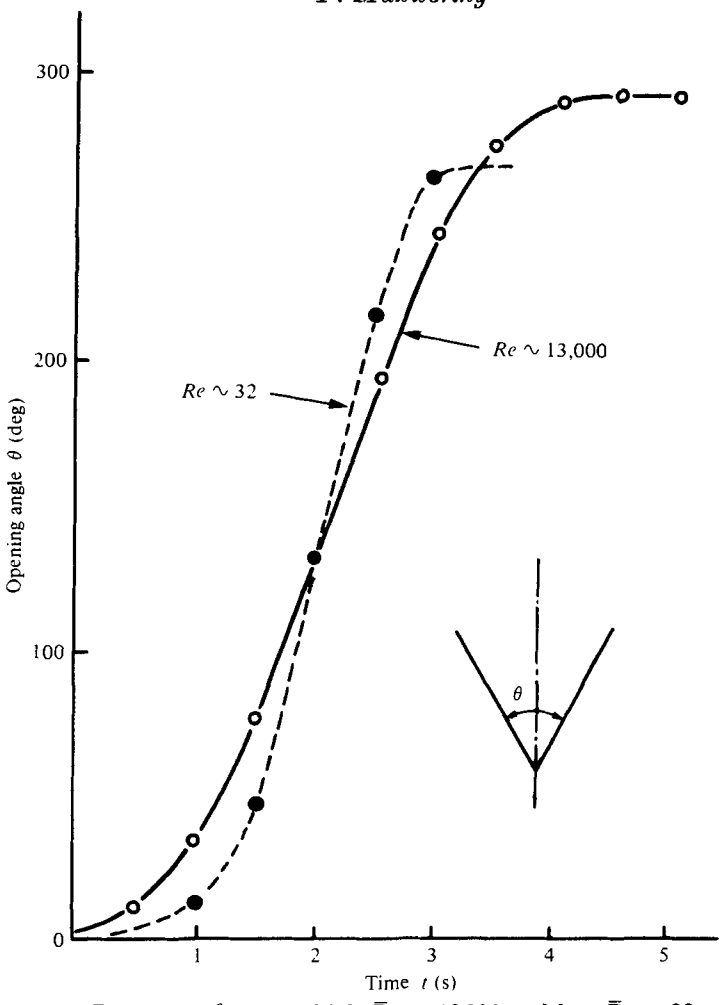

FIGURE 6. θ *vs.* t at high $\bar{R}e \sim 13000$ and low $\bar{R}e \sim 32$.

that rotate about their axes. Two horizontal rods are soldered to these vertical members and the wings themselves are attached to the former through 'Teflon' bearings so that they can rotate about the horizontal axes. Two sets of wings were made; the first was cut from 0·020 in. thick stainless steel sheet and the second from 0·030 in. Lucite sheet. Both are sufficiently light that, as the vertical rods are swivelled outwards, the resulting fluid dynamic forces push the trailing edges of the wings together to form a V. When the angle of opening (θ) reaches approximately 120°, thin rods attached to the wing axes hit 'stops' and further wing rotation is prevented. Thereafter the wings move in an arc, i.e. ϕ increasing, with a constant angle of attack until they 'flip' over at the farthest extreme of their motion.

Both models could be placed in a large Lucite container filled with either water or glycerine and the flow observed using dye or small, neutrally buoyant wax particles. By taking streak photographs of the latter using a camera with a known exposure time, one can measure the local fluid velocity and, hence, determine the circulation around the wings at any instant.

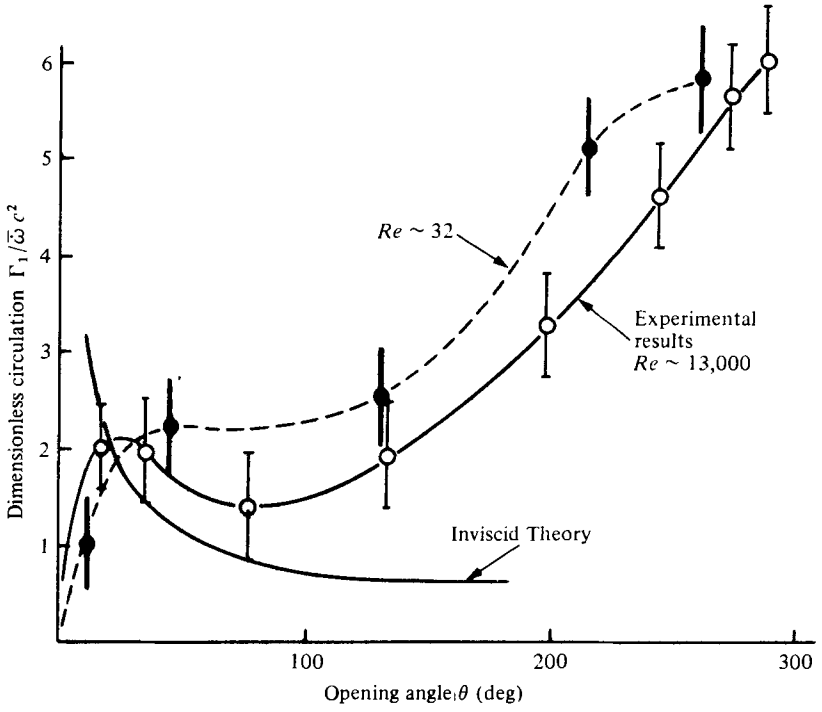

FIGURE 7. Γ_1/Γ_0 *vs.* t at high and low $\bar{R}e$. (See figure 14 for a definition of Γ_1.)

3. Results

3.1. *Experiments on two-dimensional flow over a rotating wing-pair*

Two sets of experiments were performed. The first used water as the working fluid, in order to investigate the system's behaviour at higher Reynolds numbers suitable for comparison with Lighthill's (1973) inviscid theory. From the photographs of this flow (figure 5, plates 1 and 2), it is immediately clear that a separation vortex is formed that grows bigger as the wings continue to open as suggested in § 3 of Lighthill (1973). However, it is also clear that the major part of the circulation created by the wing motion is contained within these vortices. In fact, the circulation around the wing surface alone is actually of opposite sign to that in the vortex, being dominated by the vortex induced flow directed towards the wing tip on the upper surface. In figures 6 and 7, we show the angular displacement-time history and the total circulation-displacement history for this flow. In the latter we have normalized the circulation, using a mean value for the angular velocity (i.e. $\bar{\Gamma}_0 = \bar{\omega}c^2$) while the total circulation itself was measured directly from the photographs using the known exposure time to calculate the local velocities of individual particles.

We note that initially, for small opening angles, Lighthill's inviscid theory estimates the circulation reasonably well. However, after the wings have opened through 40° or so, this trend is reversed and the experiment rapidly departs from the theoretical values. This occurs because the real fluid is able to accumulate vorticity within the separation vortex, while in the inviscid model the intense vortex sheets created initially are actually reduced in strength by the subsequent wing motion. Also the slight enhancement of circulation predicted by Lighthill [1973, (equation 14)] as a

consequence of the leading-edge separation bubble is seen to be qualitatively correct, but the quantitative effect observed is much greater. Differences must also result because the idealized wing motion takes place at constant angular velocity, requiring an infinite torque initially, whereas the wings in any real experiment must accelerate and decelerate to and from a constant speed over a reasonable fraction of their total angular motion. In the fling stage of the Weis-Fogh mechanism, as hypothesized, the wings stop rotating when they have reached an opening angle (θ) of approximately 120° at which point the measured circulation is approximately three times that estimated by the inviscid theory. In the experiment, the wings continue to open until $\theta \approx 270°$, a situation that appears to be typical of the wing excursion of many butterflies. In this case, the final circulation is very large, being typically $6\bar{\omega}c^2$ to $8\bar{\omega}c^2$ depending on the final angle chosen. We will use this result in the appendix in order to estimate the lift force on such insects under one particular set of circumstances.

Both the theoretical and experimental results given above are appropriate for flight at large *Re*. However, most estimates for the 'clap and fling' mechanism, at least, place a value between 20 and 200 on this parameter under which circumstances our estimates are likely to be in error. In order to remove any doubts on this point, we have repeated these experiments in a very viscous fluid, glycerine, and show these results in figure 6, 7 and 8 (plate 3). Even at $Re \approx 32$, we see from figure 8 that a substantial separation vortex still exists and that the total circulation is still dominated by its presence. Several details are of interest. At small opening angles the circulation is small, when normlaized with the mean reference circulation $\bar{\omega}c^2$, because the initial opening rates are small and Γ_1 must start from zero in this case.† The same trend is also apparent in the high *Re* data although the trend of the inviscid theory is apparently followed to a larger angle. If the data were normalized with the instantaneous value of the opening rate rather than the average value, one would expect and, in fact finds, a closer agreement. However, the average opening rate is the more useful value to use in this case (see § 4). Also at low *Re* the normalized circulation is genearally larger than that at high *Re*, a result for which we have no explanation at the moment, except to note that the same trend with *Re* is found during the formation of vortex rings from an orifice (Maxworthy 1977).

3.2. *Experiments on the three-dimensional flow created during the 'fling' process*

In nature, the fling process apparently occurs only at low *Re*, and so we concentrate here on the experiments performed with the model shown in figure 4 placed in the tank filled with glycerine. However, initially we have experimented with the same model in water using both dye and particles to observe the fluid motion and this has given a better appreciation of some of the complex motions that can occur and was very useful in interpreting the glycerine experiments which could be visualized using only the particle technique.

In figures 9*A* (plate 4) and 10 (plate 5) we show a series of photographs taken during one cycle of the fling process using a thin light plane to illuminate the particles. In figure 9*A* the light beam was located in a plane that was perpendicular to the initial position of the horizontal axes of the wing-pair and cut the transparent wings

† In fact in these experiments it proved to be impossible to start the motion with θ zero because the wings would not open (and also remain stable) within a reasonable time.

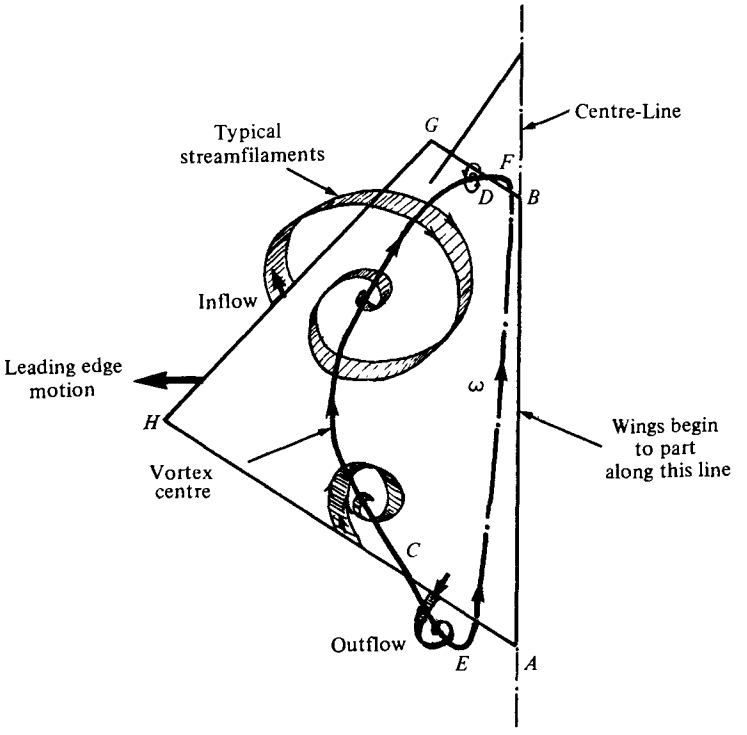

FIGURE 11. Sketch of vortex flow over one wing during the initial phase of the fling. The total flow is symmetric about the centre-line.

at a line midway between the front and back edges (see figure 4 *e*). In figure 10 the light plane cuts the wing plane at the back edges of the wings (see figure 4 *e*). From such photographs and many hours spent observing particle and dye motion and then reconstructing and sketching vortex motion, we present the following composite picture of the total flow field, although there are still some subtleties that cannot be resolved completely.

We start the motion with the wings pressed together, as in figure 4 *a*. As the horizontal arms begin to rotate, the hydrodynamic forces acting on the wings are such that their bottom edges remain in contact and the wings form a continually opening V as in figure 2. Fluid rushes into and out of the opening gap and flow separation occurs at all exposed edges. At the point of maximum opening, the vortex structure is as drawn crudely in figure 11 and a two-dimensional slice, figure 9 *A*, (*a*)–(*c*), is different from that shown in figures 5 and 8 for the two-dimensional experiment. We see that a second vortex pair is created below the wing surfaces and that it must detract from the overall lift created by separation at the leading edge.

We also note that the flow at this stage is different from that at the same opening angle, but at high *Re* (figure 9 *B*, *a*–*c*). In the latter case, the vorticity under the V has not concentrated into a vortex, but remains attached closely to the lower wing surface, although its contribution to the total circulation is also negative. At low *Re* either separation and/or diffusion occurs on such a scale that an identifiable vortex is formed. This result is enough for us to suspect that the insect probably tries to avoid such an inefficient situation and that the leading edge motion in reality is such that

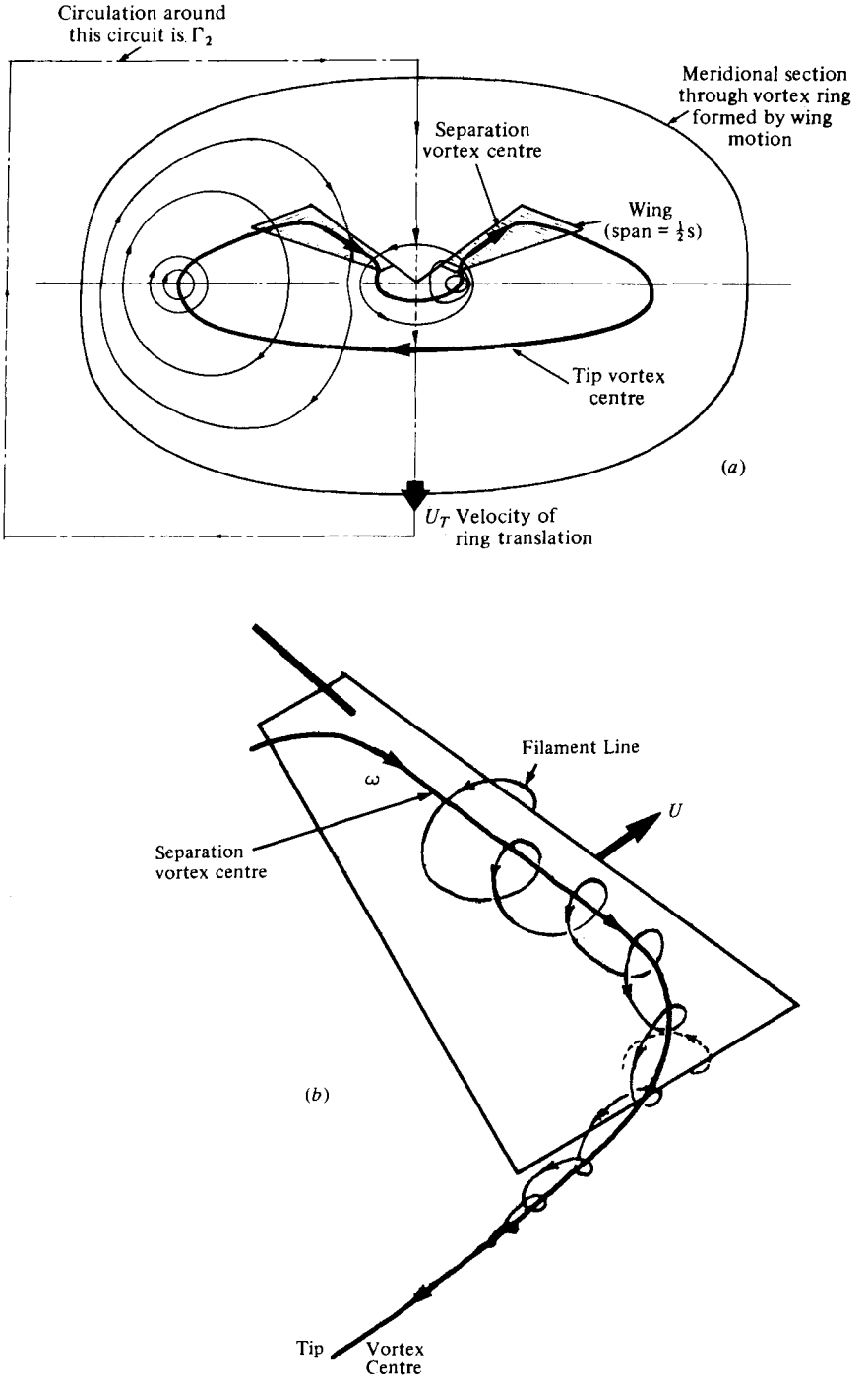

FIGURE 12. (*a*) Sketch overall flow field at the instant before the wings 'flip' over at the extreme of their motion. Showing the large vortex ring formed by the combined tip vortices. (*b*) Sketch of the flow over the wing during the quasi-steady second phase of the fling showing the axial flow in the separation vortex that feeds vorticity into the tip vortex.

it moves downwards as the wing opens in order to approximate the two-dimensional flow more closely. From the subsequent pictures it is also clear that this vortex is only of importance during the initial phase of the fling and that no more vorticity appears to be fed into it once the wing rotation stops and the trailing edges part. As the motion continues and the trailing edges do begin to part (at AB in figure 11), the relatively weak vortex ends at E and F appear to join up with the 'image' vortex on the other wing.† At the same time a developing three-dimensional motion over the upper surface of the wing causes the main vortex (CD) to be displaced along its axis to join up with the corresponding vortex on the other wing to create an outer 'tip' vortex (at AH in figure 11) of more or less uniform circulation spanning the gap between the wings. At the same time, vorticity is continuously being created and separated at the leading edge to eventually form a quasi-steady separation bubble over the wing (figure 12*a*, *b*; figure 15) within which the flow is three-dimensional with a strong flow component along the axis of the vortex that removes vorticity from the neighbourhood of the wing and into the tip vortex (figure 12*b*). This condition continues until the wing axes reach the extremes of their motion (figure 12*a*) at which time the wings 'flip' over, reverse direction and acquire circulation of the opposite sign. The details of this motion are beyond the scope of the present paper except to note that the 'flip' process is necessary to ensure the ultimate downward motion of the total vortex pattern. This process is shown in figure 13 (plate 6) where we see that the original bubble on the top surface of the wing is forced below the wing by the 'flip' and moves downwards. Had the 'flip' not occurred and had the vortex remained on the top surface, its ultimate motion would have been upwards, representing a negative lift over this last portion of the wing motion. The final result of this cycle of wing motion is, thus, two vortex rings. A larger downward moving one with a major diameter, to the centres of rotation, of the order of the insect's total wing span (figure 12*a*) and a smaller, upward moving one that comes from the trailing vorticity shed at the inner wing tip (BG). The larger vortex is actually slightly tilted because the vorticity closest to the reader in figure 12*a* has been formed earlier and has had slightly longer to move downward. The smaller vortex is only shown diagrammatically because it becomes very distorted under the straining field of the larger and rapidly loses a clear identity. However, the application of elementary vortex dynamics leads to the conclusion that these vortex elements must exist somewhere in the flow and that the force required to produce them must detract slightly from the force responsible for the larger vortex. As pointed out in the following section, and Lighthill (1973), the total impulse of this system represents the integrated effect of the force acting on the fluid during this period of wing motion.

4. Discussion

From the results presented in the previous section, it is evident that votex motion and, in particular the motion of vortex pairs and rings, must be a central concern in any description of the dynamics of hovering flight. By way of introduction to this section,

† Because of the difficulty of determining the vortex motion unambiguously so close to the wing root it is not clear whether or not the ends of these vortices actually join up with trailing vortices from the inner 'wing' tips (BG in figure 11) to form a complex, contorted vortex filament that lies both above and below the wing surfaces.

we briefly review the appropriate ideas. The crucial concept is that of the fluid impulse, as indeed was pointed out by Lighthill (1973) in his figure 8 and the lines following it,

$$\mathbf{I} = \tfrac{1}{2}\rho \int \mathbf{x} \times \boldsymbol{\omega}\, dV,$$

where $\mathbf{x}$ is the position vector of the element of volume in question and the integral is in principle taken over the whole fluid volume but clearly need be taken over only that volume within which the vorticity, $\boldsymbol{\omega}$, exists. This impulse is created by forces acting on the fluid in such a way that

$$\mathbf{I} = \int_0^T \mathbf{F}(t)\, dt,$$

where T is the total time during which the force, $\mathbf{F}$, acts. In the present case it is immediately apparent from these two ideas that any vortices that are produced are the result of the forces created by the wing motions and that the impulse of these vortices in both magnitude and direction can be used as a measure of the integrated forces acting on the fluid and, by Newton's Third Law, the force acting on the wing. In particular, for greatest efficiency the insect must strive to produce vortices that always move downwards since any motion that forms vorticity moving upwards represents negative lift and, hence, a loss of altitude. As we have seen, and will be explored in what follows, insects that use the 'clap–fling–flip' motions are very efficient in this regard.

It is also obvious from the description given in the previous section that the explanation given by Weis-Fogh (1973) and Lighthill (1973) is basically correct in that intense vorticity, large circulations (and as we shall see) large forces are rapidly formed by the wings motions and that Wagner effect is essentially avoided.

4.1. *Model of the initial phase of the fling*

In figure 14 we show a section through the wing pair at a distance x from the root at the moment when the wings begin to part at the apex of the V and the angle between the wings (θ_f) is about 120°. To fix ideas and ease the algebraic manipulations we will assume that the wings have a triangular plan form [figure 14 and as in Weis-Fogh (1973), figure 13], that the flow field is conical and that at each x station the flow is locally two-dimensional. As a result

$$c = 2c_0(x/s), \quad L = 2L_0(x/s) \quad \text{and} \quad \Gamma_1 = 4\Gamma_0(x^2/s^2), \tag{1}$$

where the subscript '0' refers to maximum values at the end of the wings, i.e. $x = \frac{1}{2}s$, and $\Gamma_1(x)$ is the final circulation.

The final impulse residing in this vortex system when $\theta_f = 120°$, is

$$I_1 = \rho \int_0^{\frac{1}{2}s} \Gamma_1 L\, dx \tag{2}$$

where ρ is the fluid density and we have used the formulation in Lamb (1945) §§ 155 and 157, for concentrated two-dimensional vortices. We also assumed that the insect, in striving for maximum efficiency, does not just move its leading edges horizontally as in our experiments but that they also move downwards in order to partially eliminate the vortices below the wing surface (figure 9*A*).

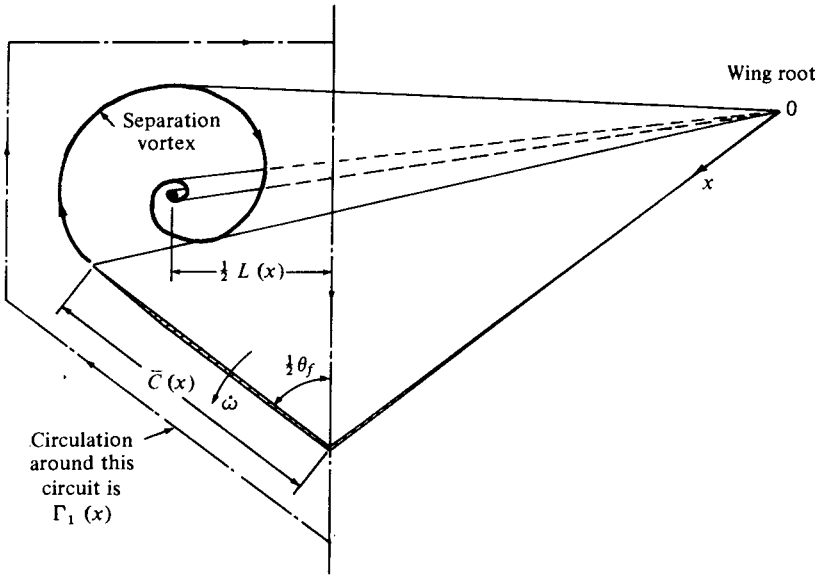

FIGURE 14. Model of the initial phase of the fling.

The impulse I_1 has been produced during a time T_1 so that the average force acting over this period of wing motion is, on substitution from (1) and integrating

$$\bar{F}_1 \approx \rho \Gamma_0 L_0 s / 8 T_1. \tag{3}$$

From figure 5*A* (*f*), $L_0 \approx \frac{5}{4} c_0$ and from figure 7 we will use $\Gamma_0 \approx 2{\cdot}5 \bar{\omega} c_0^2$. Finally we need to calculate $\bar{\omega}$, which for an opening angle of 120° becomes $\pi/3T_1$.

Substitution into (3) gives

$$\bar{F}_1 \approx 0{\cdot}41 \rho s c_0^3 / T_1^2. \tag{4}$$

From Weis-Fogh (1973) $s \approx 1{\cdot}2\,\text{mm}$, $c_0 \approx 0{\cdot}4\,\text{mm}$ and $T_1 \approx 2/7000 s$ for which $\bar{F}_1 \approx 3{\cdot}8 \times 10^{-5}$ g. Additionally we should include the impulse created at the wing tips over a distance of approximately c_0 (i.e. along AH in figure 11). For this we estimate an average force of $0{\cdot}6 \rho c_0^4 / T_1^2$ so that this contributes 50% additional lift for an insect with the dimensions of *Encarsia formosa*. The total lift generated during this phase is therefore $\bar{F}_1^* \approx 5{\cdot}7 \times 10^{-5}$ g. Since the insect weight is approximately $2{\cdot}5 \times 10^{-5}$ g, we see that our estimate is comfortably in excess and allows for any loss of lift that will arise from interactions with previously produced vorticity, deviations from local two-dimensionality, a non-triangular planform, wing flexibility etc.

In order to calculate an effective lift coefficient we need to calculate a reference force which for our present system becomes

$$F_{\text{ref}} = 2 \int_0^{\frac{1}{2}s} \tfrac{1}{2} \rho u^2(x)\, c(x)\, dx, \tag{5}$$

where the velocity of the wing leading edge during the total opening process is $u = 2u_0(x/s)$, so that $F_{\text{ref}} = \frac{1}{8} \rho u_0^2 c_0 s$. Furthermore we will assume based on Weis-Fogh (1973) that the wings open fully from $\phi = 0$ to 135° in a time T_2 to give

$$u_0 \approx \tfrac{3}{8} \pi s / T_2 \quad \text{and} \quad F_{\text{ref}} \approx 0{\cdot}17 \rho s^3 c_0 / T_2^2. \tag{6}$$

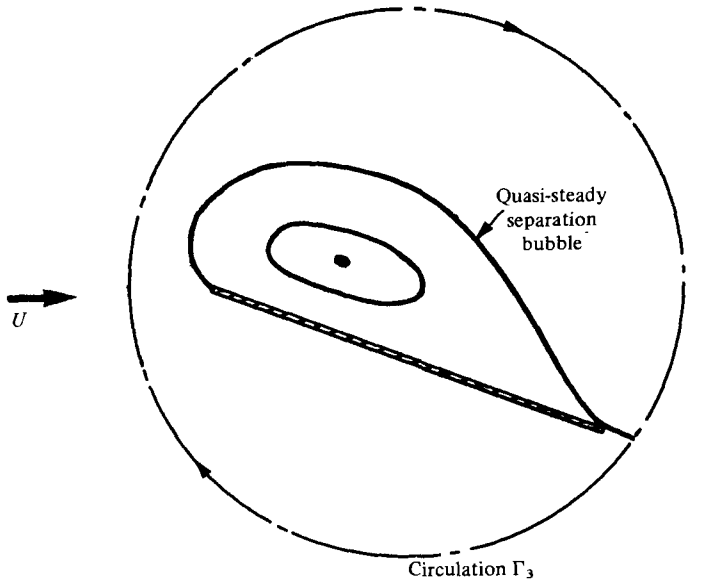

FIGURE 15. Model of the quasi-steady flow during the second phase of the fling. Showing the separation bubble that moves with the wing and is responsible for the majority of the lift.

Finally the estimated lift coefficient becomes

$$c_{F_1} = \frac{\bar{F}_1^*}{\bar{F}_{\text{ref}}} \approx 3{\cdot}6\frac{c_0^2}{s^2}\cdot\frac{T_2^2}{T_1^2} \quad \text{and since} \quad T_2 \approx \tfrac{9}{7000}s, \quad c_{F_1} \approx 8{\cdot}1.$$

4.2. *Models of the total fling process*

(*a*) *Vortex ring representation.* The ultimate flow field created by the total opening motion of the wings is as sketched in figure 12 (*a*). For the larger vortex ring we estimate the impulse to be

$$I_2 \approx 0{\cdot}51\rho s^2\Gamma_0, \tag{7}$$†

where Γ_0, the maximum value of the circulation around the wing, enters the trailing vortex ring system at the outer wing tip (see Lighthill 1973, figure 8). Since little vorticity appears to be lost or gained during the transition from the initial fling to the quasi-steady opening motion we have further assumed that this value of the circulation is the same as that in § 4.1 and that the vorticity left on the wing completes the total vortex ring. In this formulation we have assumed that the distance between the centres of rotation within the vortex is 0·9*s* and have used the results quoted in Lamb (1945) § 165 for a Hill's spherical vortex.†

This impulse is produced by a force $\bar{F}_2$ acting for a time T_2 and hence on substituting for Γ_0

$$\bar{F}_2 \approx 1{\cdot}3\rho\frac{s^2c_0^2}{T_1T_2}. \tag{8}$$

Using previously stated values for the insect dimensions and flapping periods gives

$$\bar{F}_2 \approx 8{\cdot}1\times10^{-5}\text{ g}.$$

† Using a concentrated vortex model gives $I_2 \approx 0{\cdot}64\rho s^2\Gamma_0$ and presumably more realistic vortex distributions will give an impulse of about these values.

From this we must subtract the negative contribution of the inner vortex ring for which we estimate the diameter to the centres of rotation to be $0{\cdot}4s$. This force is $\bar{F}_{2_i} \approx 0{\cdot}2\rho s^2 c_0^2/T_1T_2$ since its circulation is identical that around the larger vortex ring, and we finally obtain a total lift of $\bar{F}_2^* \approx 1{\cdot}1\rho s^2 c_0^2/T_1T_2 = 6{\cdot}9 \times 10^{-5}$ g. Using (6) as the reference lift force, we obtain a lift coefficient of

$$c_{F_2} \approx 6{\cdot}5 \frac{c_0}{s} \cdot \frac{T_2}{T_1} \approx 9{\cdot}7. \tag{9}$$

(*b*) *Alternative quasi-steady lift model.* At first sight it seems that we should be able to calculate the mean lift using slightly different ideas since it is associated with the flow over the large, quasi-steady separation vortex that moves with the wing (figures 12*a*, *b*, 15).

It is obvious from very elementary arguments that in order for this quasi-steady, separation-vortex to exist, the total flow field must be three-dimensional with the vorticity created by separation at the leading edge being removed by axial flow along the vortex lines.†

In this way, a steady vortex can be formed over the wing with the axial flow feeding the excess vorticity into a tip vortex.‡ This is exactly the state of affairs in the present problem (see figure 12*b*) and the lift for our assumed wing planform is represented by:

$$\bar{F}_3 \approx 2\int_0^{\frac{1}{2}s} \rho\Gamma u\, dx = \tfrac{1}{4}\rho\Gamma_0 u_0 s, \tag{10}$$

which upon substitution for Γ_0 and u_0 gives

$$\bar{F}_3 \approx 0{\cdot}77\rho s^2 c_0^2/T_1T_2 \approx 4{\cdot}8 \times 10^{-5}\,\text{g} \tag{11}$$

and

$$c_{F_3} \approx 4{\cdot}5 \frac{c_0}{s} \cdot \frac{T_2}{T_1} \approx 6{\cdot}8. \tag{12}$$

These values are approximately 75 % of those calculated from the previous model, partly because we have ignored unsteady effects and, especially, the impulse associated with the production of the 'starting' vortices and, partly because of the general inaccuracy of these estimates. In any case the forces based on any of these models are far in excess of those needed for the insect to balance its weight and there is sufficient overproduction of vorticity to allow for many of the important interference effects that will tend inevitably to reduce the available final impulse.

Finally, based on some preliminary experiments it appears that the 'clap' phase of the wing motion generates an even larger lift-force than the initial phase of the fling so that the combined clap and fling is an extremely effective way of continuously producing vorticity of the correct sign and at no stage produces substantial amounts that move in the wrong direction.

† In the strictly two-dimensional case such vorticity is removed by an unsteady shedding mechanism, as in the 'Kármán vortex street', and is very inefficient at promoting a steady lift.

‡ The arguments here are similar to those required to rationalize the large lift coefficients attained by 'delta' wings at large angles of attack where leading edge separation vortices with axial flow account for a significant fraction of the total lift.

My interpretation and understanding of the experimental results were greatly aided by discussion with Professor Sir James Lighthill and C. P. Ellington at Cambridge University, Professor Philip Saffman at the California Institute of Technology and Professors H. K. Cheng and Richard Edwards at the University of Southern California. Their help is gratefully acknowledged.

Appendix. Modelling of some aspects of Butterfly dynamics

We are now in a position to make some simple estimates of the lift force acting on butterflies for at least one clear-cut circumstance. In this we have been guided not only by personal observations, but especially by some very revealing sequences presented in a fascinating film by C. P. Ellington and G. G. Runnells of Cambridge University entitled 'High speed research films of free flying insects'. The latter in particular reveals clearly the subtleties introduced into the dynamics by wing flexibility. As a result, basically simple motions often evolve through a sequence of states that might be interpreted quite differently by different observers. In one particular sequence a Cabbage White is shown taking-off from rest by apparently performing a modified version of our two-dimensoinal experiment. The wings start pressed together but, because of wing flexibility, as the wings rotate about the insect's body axis the leading edges do not open uniformly (as in our experiment), and so the motion can also be described as a rotation about the wing trailing edges.† The wings then continue opening through almost 360° until they clap in the ventral position. In the spirit of our models presented in § 4 we can estimate the order of magnitude of the forces involved in this case and show how it can result in one explanation of the very dramatic vertical motion of the insect observed in the movie sequence. We assume that the butterfly has a wing of retangular planform with a span r‡ and a length l.‡ Taking account of the vorticity produced at all exposed edges as in § 4.1 we estimate the final average force to be

$$\bar{F}_B \approx (\rho \Gamma_B r/T_B)(l+\tfrac{1}{8}r),$$

where Γ_B is the final maximum circulation, T_B the time taken for the wings to open and we have assumed the distance between the vortex centres of rotaion to be r. From an extrapolation of the curves of figure 7 we can estimate

$$\Gamma_B \approx 8\left(\frac{r}{2}\right)^2 \bar{\omega}_B \quad \text{when } \theta_f \approx 360°$$

and since

$$\bar{\omega} \approx \pi/T_B, \quad \bar{F}_B \approx \frac{2\pi\rho r^3}{T_B^2}(l+\tfrac{1}{8}r).$$

For $r \approx 4$ cm, $l \approx 3$ cm and $T_B \approx 0{\cdot}03$ s this results in a lift force of 1·6 g and thus, for insect weighing about 0·2 g a vertical acceleration of 8 g and a vertical rise of 3·5 cm. In the movie the rise is around $\frac{1}{2}r$ or 2 cm for our example! Unquestionably our estimate is too large because among other things, we have ignored the effect of this vertical rise on the formation of vorticity at the wings edges.

† As pointed out by a referee. We are also grateful to this same referee for re-focusing our attention on this particular sequence with the result that the present estimate was undertaken to replace one of unproven validity.

‡ These correspond to $2c$ and $\frac{1}{2}s$ respectively, in the previous models.

In attempting to analyse the formation of net lift by a continuous flapping we are faced with many more interpretational difficulties mainly because the movie sequences show a variety of motions depending on the orientation of the insect body as it performs a number of gyrations. Again wing flexibility appears to play a vital role in modifying the negative lift generated as the wings perform their return or upstroke. By making suitable assumptions it is possible to estimate these forces and actually calculate a net lift that balances the insect weight. Unfortunately, the details are sufficiently problematical to require further observations before they can be set down to print.

Note added in proof 26 April 1979. During recent correspondence with C. P. Ellington of Cambridge University he has brought to my attention two papers (Ellington 1978) that have much in common with the work presented here, especially the emphasis on vortex motions created by insects in hovering flight. He has also pointed out a paper by Bennett (1977) on a two-dimensional experiment in which the wings are rotated, as in my first experiment, and then pulled apart at angle of attack. The resulting observation of a rapid decrease in lift when the wings are parted points, I believe, to the critical role played by three dimensional effects in removed vorticity produced by leading edge separation in the present experiments. In Bennett's experiments such vorticity can only be lost by a dramatic shedding of all the accumulated vorticity with a concommitant loss of lift, as pointed out in the footnote on page 61 of this paper.

REFERENCES

BENNETT, L. 1977. Clap and fling aerodynamics – an experimental evaluation. *J. exp. Biol.* **69**, 261–72.

ELLINGTON, C. P. 1975 Nonsteady aerodynamics of the flight of *Encarsia formosa*. In *Swimming and Flying Nature*, vol. 2 (eds. T. Y. Wu, C. J. Brokaw & C. Brennen). New York: Plenum Press.

ELLINGTON, C. P. 1978 The aerodynamics of normal hovering flight: three approaches. In *Comparative Physiology – Water, Ions and Fluid Mechanics* (eds. Schmidt-Nielsen, Bolis and Maddrell). Cambridge University Press.

ELLINGTON, C. P. 1979 Vortices and Hovering Flight. *Proc. Conf. Unsteady Effects of Oscillating Insect Wings* (Ed. W. Nachtigall). In press.

LAMB, H. 1945 *Hydrodynamics*, 6th ed. New York: Dover.

LIGHTHILL, M. J. 1973 On the Weis-Fogh mechanism of lift generation. *J. Fluid Mech.* **60**, 1-17.

LIGHTHILL, M. J. 1975 Aerodynamic aspects of animal flight. In *Swimming and Flying in Nature*, vol. 2 (eds. T. Y. Chu, C. J. Brokaw & C. Brenner) New York: Plenum Press.

MAXWORTHY, T. 1977 Some experimental studies of vortex rings. *J. Fluid Mech.* **81**, 465–495.

WAGNER, H. 1925 *Z. angew. Math. Mech.* **5**, 17.

WEIS-FOGH, T. 1973 Quick estimates of flight fitness in hovering animals including novel mechanisms for lift production. *J. exp. Biol.* **59**, 169–230.

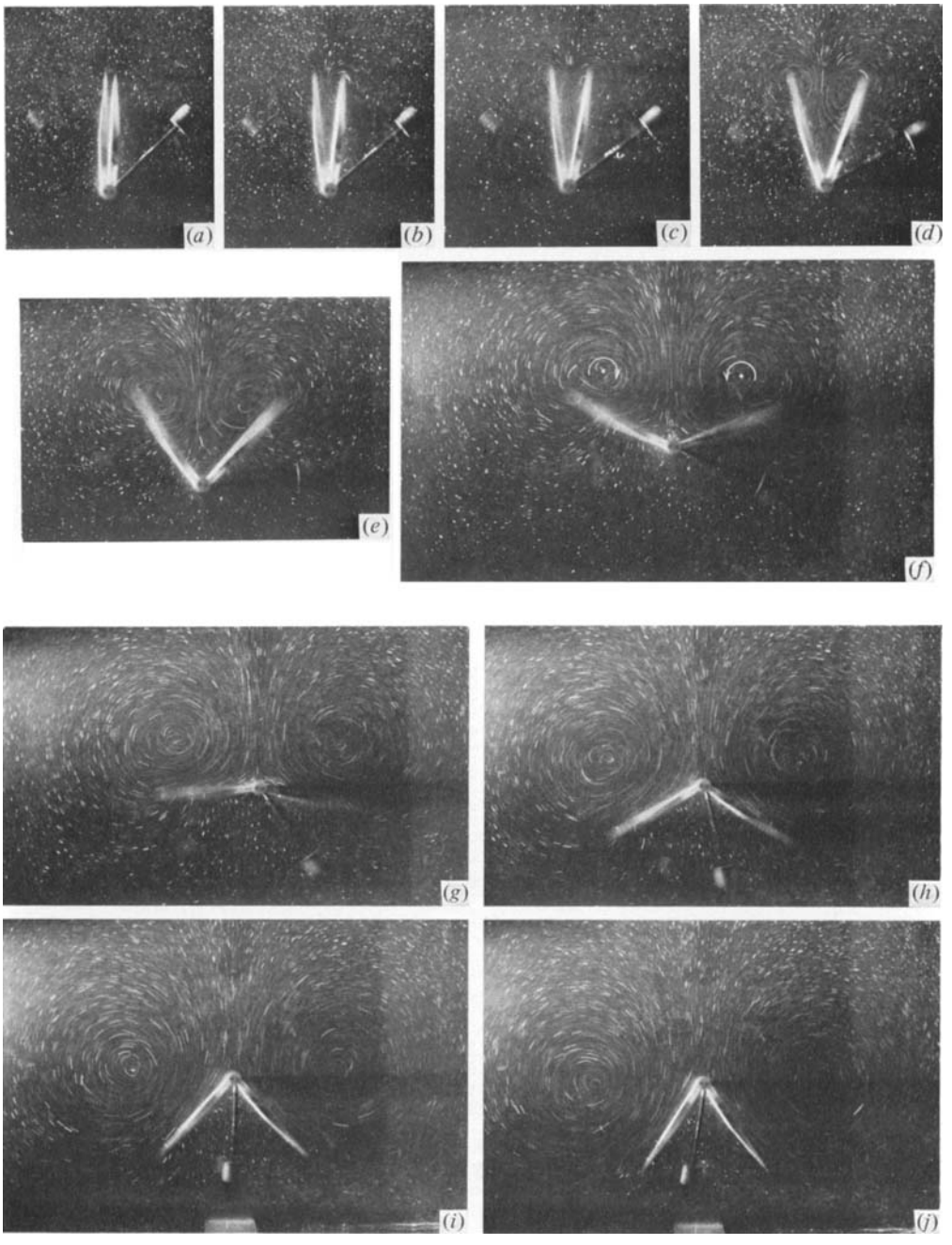

FIGURE 5. (*A*) Particle streak photograph of two-dimensional flow over rotating wings. The dominant presence of the separation vortices is apparent. Time between photographs is about 0·5 s, camera exposure time about $\frac{1}{16}$ s, $\bar{R}e \approx 13000$.

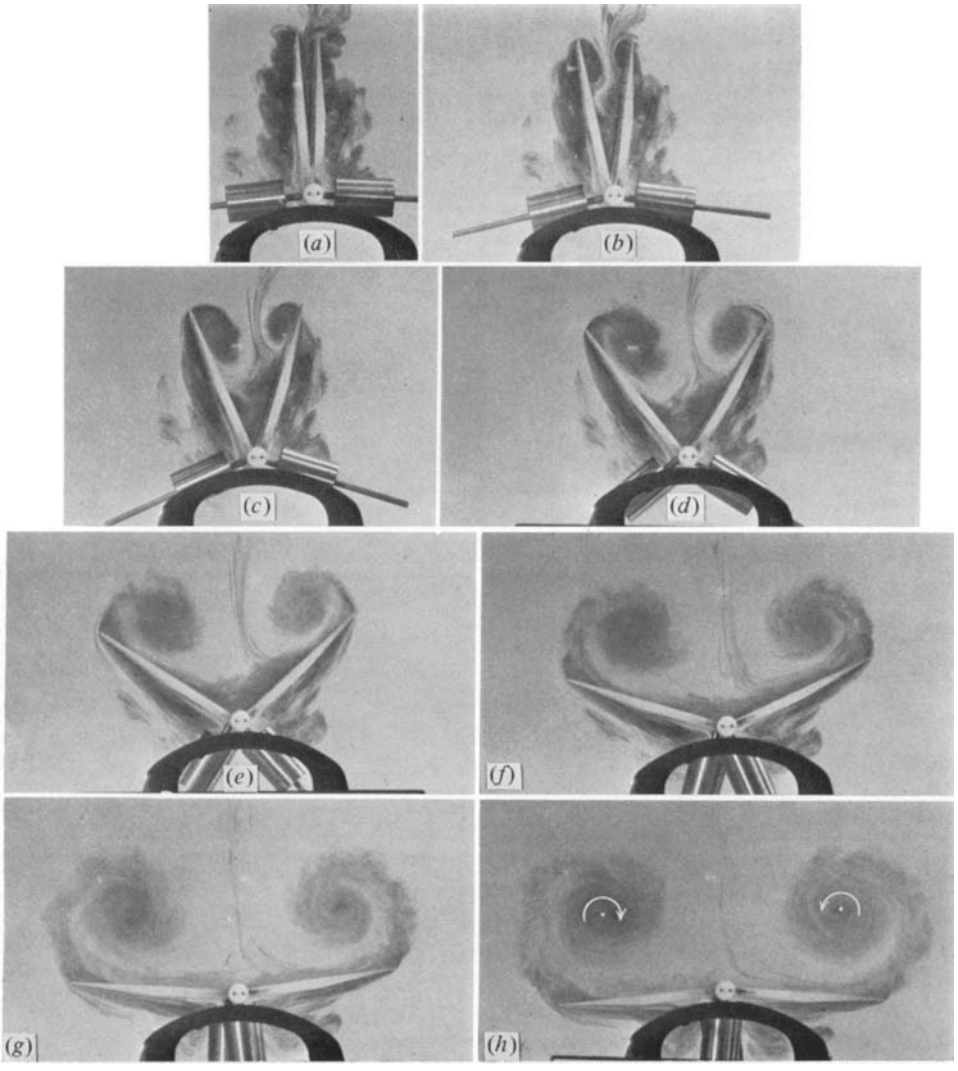

FIGURE 5(*B*). Dye photograph of the two-dimensional flow over rotating wings. $\bar{R}e \approx 13000$. Note the interior vortex created by boundary layer separation initially but which gains no vorticity during the subsequent wing motion.

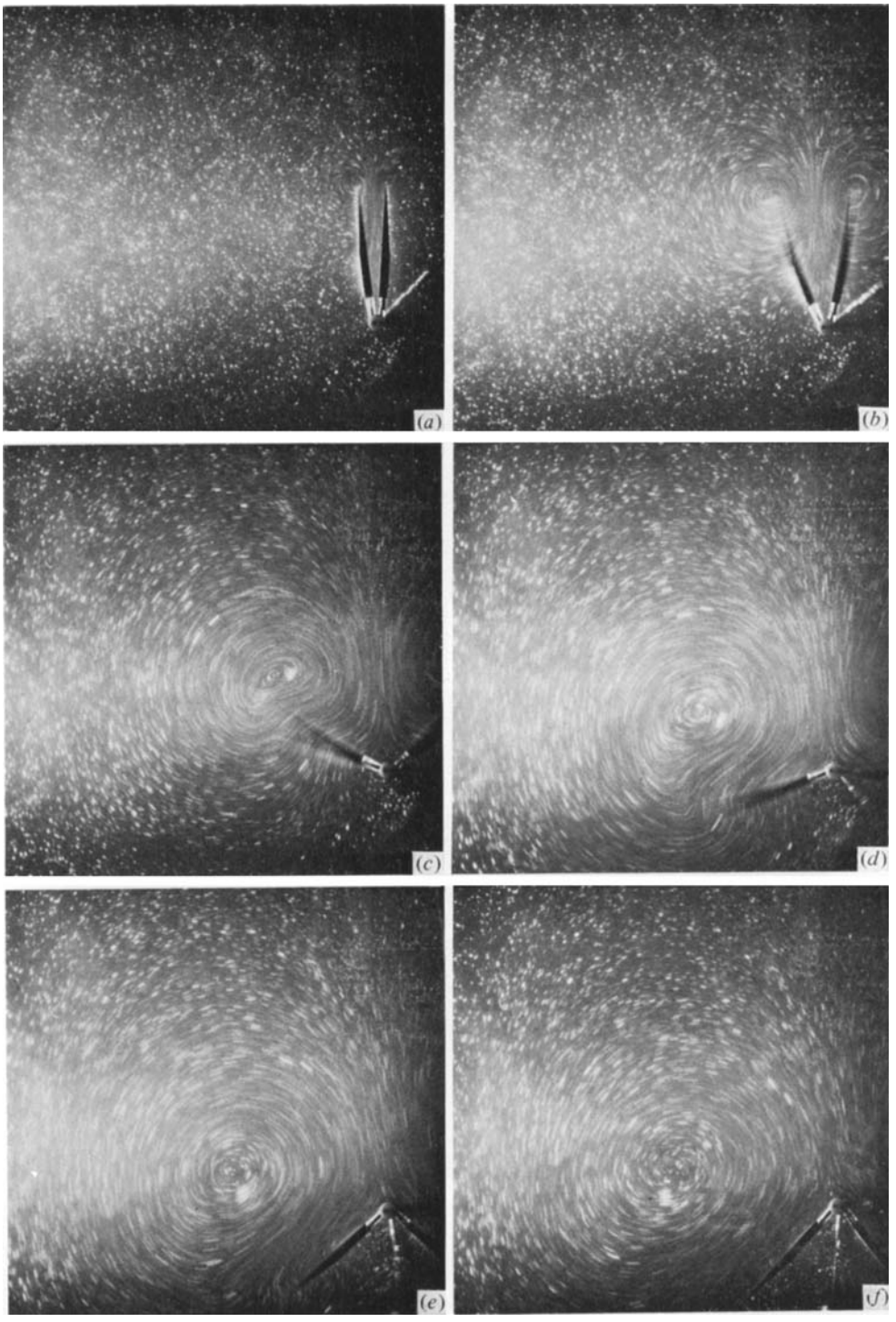

FIGURE 8. Same as figure 5(*A*) except at low $\bar{R}e \approx 32$. Exposure time $\sim \frac{1}{3}$ s.

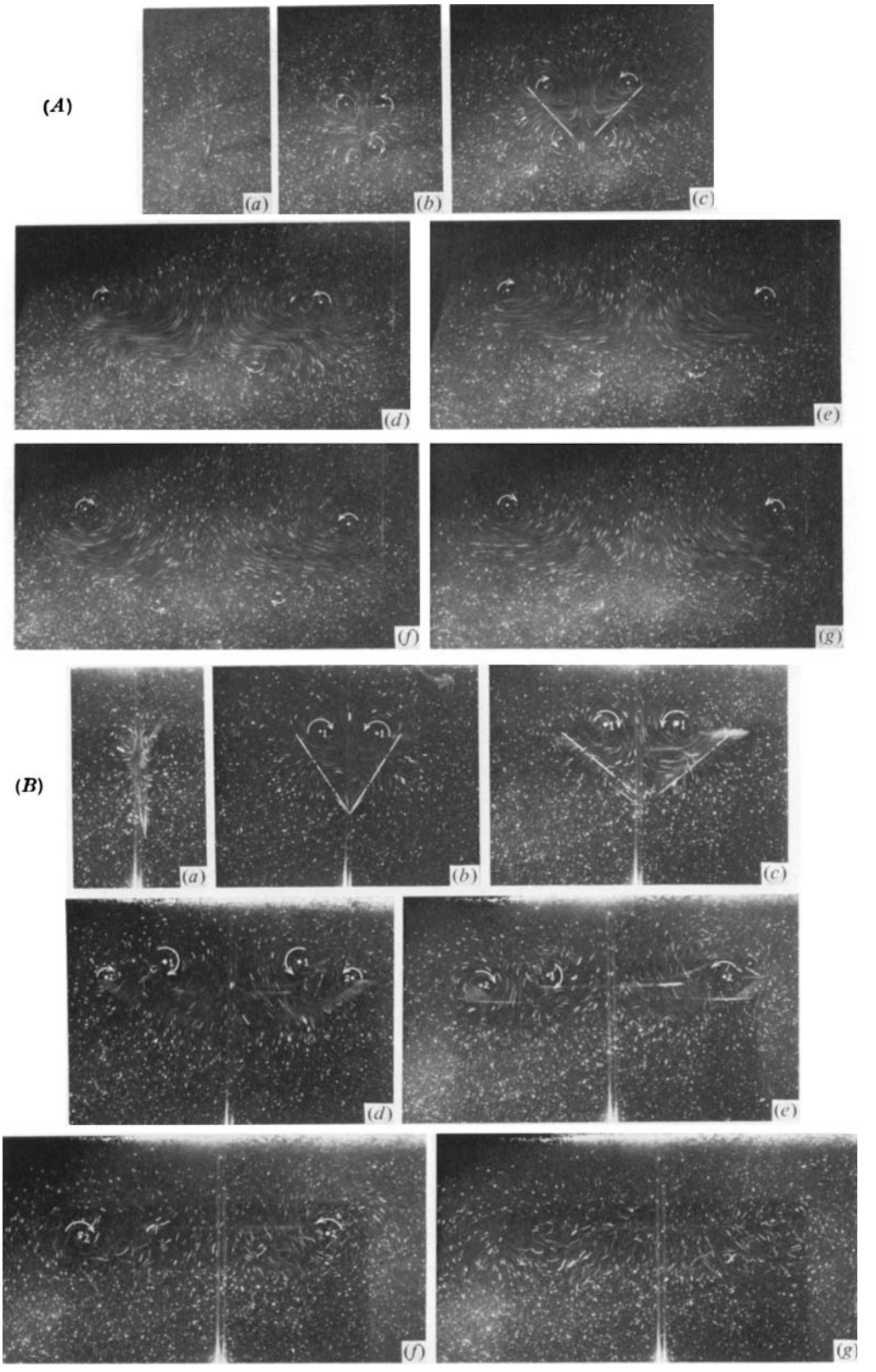

FIGURE 9 (*A*) and (*B*). For legend see facing page.

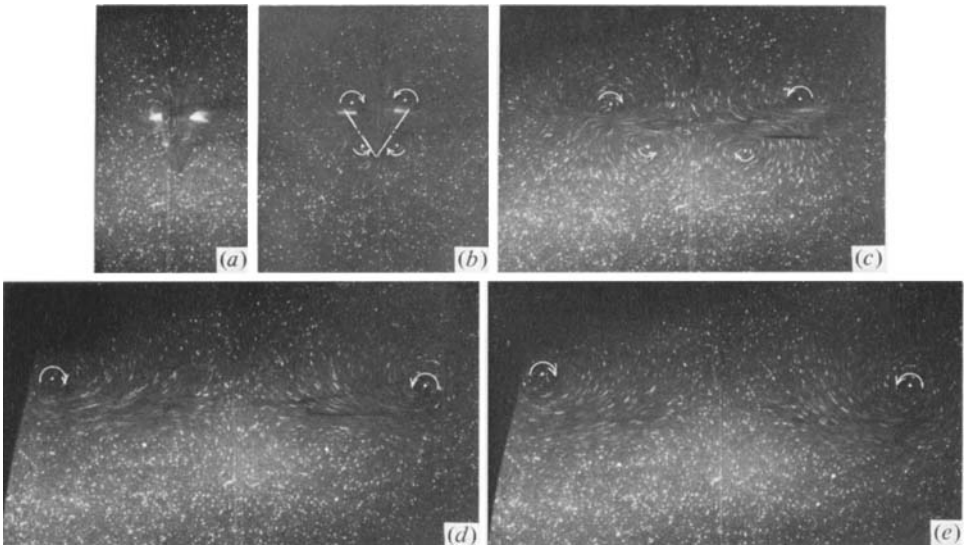

FIGURE 10. Same as figure 9(*A*) except the light slice is located at the back edge of the wings (figure 4*e*). This view gives the best idea of the final location of the tip vortices and the diameter of the vortex ring that is formed (see figure 12*a*).

FIGURE 9(*A*) Streak photographs of three-dimensional fling process using a light slice at the wing mid plane (figure 4*e*) at low *Re*. The directions of vortex motion are indicated as are the positions of the wings. The formation of separation vortices above the wings and secondary vortices below is clear as is the transition of the separation vortex to a tip vortex as the motion proceeds. The outline of the wings, outside the plane of the light beam, is visible in the last few pictures. (*B*) Same as figure 9(*A*) except a high *Re*. The secondary vortices below the wings are absent. Also the initial separation vortices, (1), are not incorporated into the tip vortex but are actually shed downwards between the wings to produce a flow rather different and more complex than that found at low *Re*. Note the appearance of new quasi-steady separation vortices, (2), after the original ones (1) have separated from the wing surface.

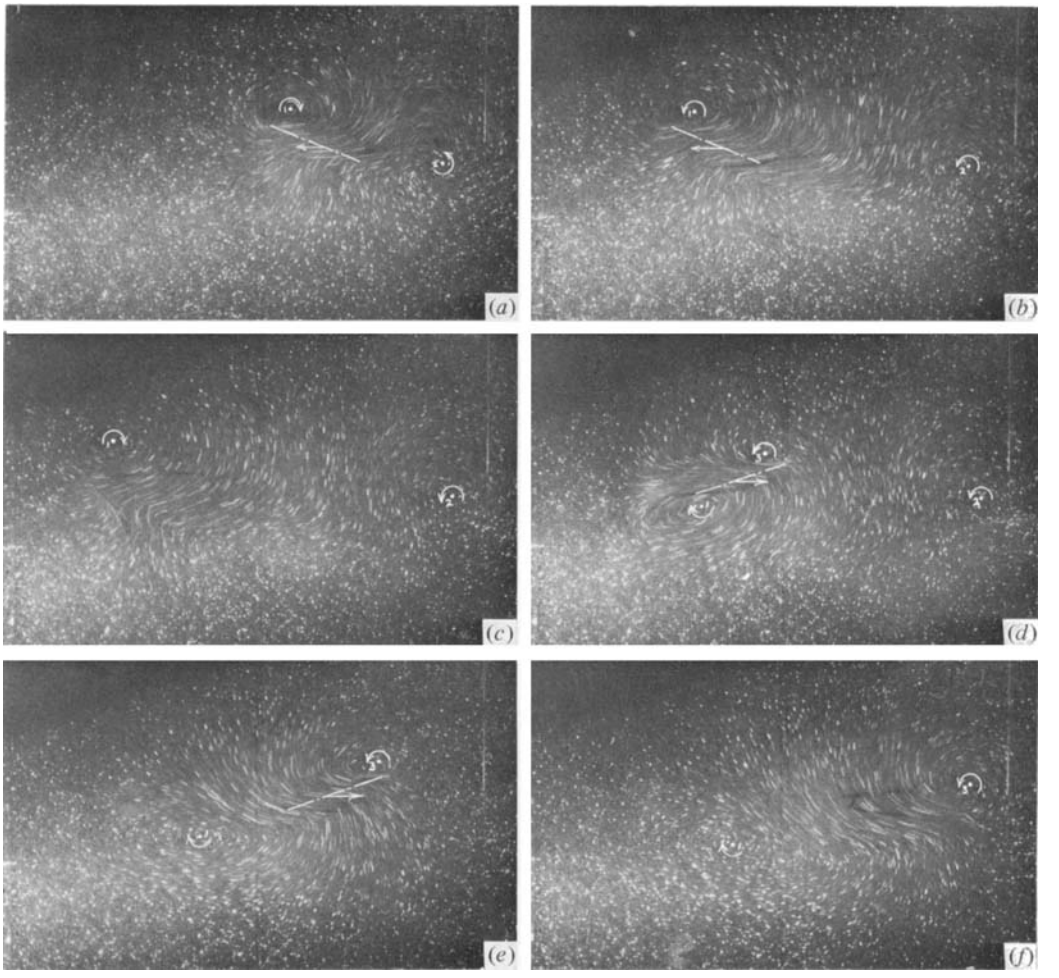

FIGURE 13. Mid slice through the wing during the flip motion. The separation vortex (1) is forced beneath the wing on the return stroke, and the new separation vortex (3) becomes the tip vortex that replaces that present originally (2).